Tanguy Mertens

A new mapped infinite partition of unity method for convected acoustical radiation in infinite domains.

January 20, 2009

Université Libre de Bruxelles

Remerciements

Si tu donnes un poisson à un homme, il ne mangera qu'un jour. S'il apprend à pêcher, il mangera toute sa vie.

Proverbe de Confucius, repris plus tard par Dominique Pire dans le cadre de l'action Iles de Paix.

Je remercie Philippe Bouillard de m'avoir donné ma canne à pêche et conduit à l'étang. Je remercie Laurent Hazard et Guy Paulus pour tous leurs conseils avisés. Et tous les autres, famille, amis, qui ont gardé confiance en moi et m'ont encouragé à la persévérance.

C'est grâce à vous tous que je peux vous présenter avec fierté mon premier poisson.

Ceci dit, je voudrais remercier de manière plus académique tous les acteurs du projet.

Je remercie Philippe Bouillard qui est à la source du projet et qui a contribué à mon épanouissement scientifique durant cette aventure au sein du service BATir. Je remercie également pour leur encadrement: Guy Warzée pour sa gentillesse et sa patience ainsi que Jean-Louis Migeot pour son soutien industriel et ses remarques pertinentes.

Ce passage au service BATir a été une expérience riche sur le plan scientifique mais aussi humain. Je remercie mes collègues de l'ULB pour les relations que nous avons construites ensemble, pour les activités dans le cadre du travail ou hors des murs de l'université. Je pense évidemment à Laurent Hazard et à Guy Paulus, pour leur amitié mais aussi leur disponibilité et leurs nombreux conseils. Merci aussi à tous les membres du service des milieux continus qui ont ajouté une dimension humaine. La nature des contrats de recherche et d'assistanat est tel qu'ils furent nombreux a être passés par les murs de l'université. Je ne pourrai tous les citer mais je tiens quand même à remercier personellement Katy, Erik, Geneviève, Yannick, Louise, Dominique, Thierry, Sandrine, Bertha, David, Benoît, Peter et Kfir.

S'il est vrai qu'un travail de thèse tend à rendre le chercheur autonome, les collaborations et interactions restent importantes. Je remercie à cet égard toute l'équipe de l'Institute of Sound and Vibration Research de l'université de Southampton. Je remercie Jeremy Astley, chef du service de m'y avoir accueilli pendant un stage de six mois. Je le

remercie aussi pour l'environnement de travail de qualité qu'il m'a offert. Il est évident que la présence de Pablo Gamallo à l'I.S.V.R. a énormément contribué à l'aboutissement de ce travail de recherche. Je le remercie pour tout le temps qu'il m'a consacré, à Southampton et même par la suite lors de contacts e-mail ou lors de rencontres en conférences. Je le remercie pour l'intérêt qu'il porte à la présente étude, pour ses encouragements et pour tous ses enseignements. Mais ce séjour n'a pas été que professionellement enrichissant, je repense à l'accueil qui m'a été réservé ainsi que de nombreux excellents souvenirs qui font de ce séjour une partie inoubliable de ma vie. Je tiens donc à remercier chaleureusement pour leur amitié précieuse Vincent et Theresa, Luigi, Claire, Naoki, Rie, Sue, Lisa, Eugene, Isa, Daniel et Stéphanie, Alessandro et Emmet.

Ces quelques lignes indiquent à quel point les relations humaines ont une influence sur ma vie. Cela ne sera pas une surprise alors si je remercie les personnes pour qui je *travaille dans les avions* ou ceux qui me félicitent de mon travail, *les semaines durant lesquelles, ils n'ont pas trop entendu les avions*. Je pense bien entendu à ma famille, principalement ma maman, pour avoir fait de moi l'homme que je suis aujourd'hui et mes amis, plus particulièrement mes collocataires: Iyad, Mathieu, Quentin, Guerrick, Caroline et Florence. Merci à vous de partager mes valeurs et de colorier mon existence.

Enfin, je terminerai par remercier les deux petits rayons de soleil qui ont ensoleillé la fin de ce long parcours.

List of Symbols

Greek symbols

β : $\sqrt{1 - M_0^2}$
γ : Poisson ratio of specific heat capacities : c_p/c_v
Γ : interface separating the inner and the outer domains
ε : Error
μ : phase function $[m]$
ρ : mass density $[kgm^{-3}]$
ρ_0 : steady mean density $[kgm^{-3}]$
ρ_a : acoustic density $[kgm^{-3}]$
$\boldsymbol{\sigma}$: stress tensor $[Nm^{-2}]$
ϕ : velocity potential $[m^2s^{-1}]$
ϕ_0 : mean velocity potential $[m^2s^{-1}]$
ϕ_a : acoustic velocity potential $[m^2s^{-1}]$
$\tilde{\phi}_a$: amplitude of the harmonic acoustic velocity potential $[m^2s^{-1}]$
$\tilde{\phi}^h$: numerical approximation of $\tilde{\phi}_a$ $[m^2s^{-1}]$
$\tilde{\phi}_h^I$: numerical approximation in the outer region Ω_o $[m^2s^{-1}]$
Φ_α : shape function for the α^{th} degree of freedom
Φ_α^I : infinite shape function for the α^{th} degree of freedom
ω : angular frequency $[s^{-1}]$
Ω : domain
Ω_i : inner region
Ω_o : outer region

Arabic symbols

$\tilde{a}_n$	: normal acceleration of a vibrating wall	$[ms^{-2}]$
A_n	: normal acoustic admittance	$[m^2skg^{-1}]$
$A_{mn}^{\pm}$	: incident and reflected modal amplitude	$[m^2s^{-1}]$
c	: speed of sound	$[ms^{-1}]$
c_0	: steady mean part of the speed of sound	$[ms^{-1}]$
c_∞	: speed of sound at large distance from the source	$[ms^{-1}]$
c_p	: specific heat capacity at constant pressure	$[JK^{-1}]$
c_v	: specific heat capacity at constant volume	$[JK^{-1}]$
$dofs$	: number of unknowns of the approximation	
E	: energy flow out of a surface	$[J]$
$E_{mn}^{\pm}$	: incident and reflected modal patern	
f	: excitation frequency	$[s^{-1}]$
G	: geometric factor	
h	: mesh size	$[m]$
H	: Hilbert space	
i	: imaginary unit $= \sqrt{-1}$	
$\mathbf{I}$	: Sound intensity	$[Wm^{-2}]$
J'	: stagnation entropy	$[Jkg^{-1}]$
k	: wavenumber	$[m^{-1}]$
$k_{r,mn}^{\pm}$	: incident and reflected radial wavenumber	$[m^{-1}]$
k_B	: Boltzmann constant	$[JK^{-1}]$
$K_{z,mn}^{\pm}$	: incident and reflected axial wavenumber	$[m^{-1}]$
L_j^d	: Legendre polynomial of order d for node j	
L_s	: curve enclosing the boundary S_s	
L_v	: curve enclosing the boundary S_v	
m	: angular mode number	
$\mathbf{m}'$	: mass flux	$[kgm^-2s^{-1}]$
m_0	: radial order of the infinite element	
m_w	: mass of a molecule	$[kg]$
M_0	: mach number	
M_i	: Mapping function for node/point i	
$\mathbf{n}$	: outer normal to the domain	
n	: radial mode number	
n_d^I	: number of infinite degree of freedom	
$n\,(j)$	: size of the local approximation space at node j	
nni	: number of infinite nodes	
$nodes$	: number of nodes	
N_i	: Partition of Unity function of node i	
N_m	: number of angular modes	
N_n	: number of radial modes	
N_M	: number of reflected modes (unknown)	

p	: fluid pressure	$[Pa]$
p_0	: steady mean fluid pressure	$[Pa]$
p_a	: acoustic pressure	$[Pa]$
$\tilde{p}_a$	: amplitude of the harmonic acoustic pressure	$[Pa]$
$\tilde{p}_{an}$	: analytic amplitude of the harmonic acoustic pressure	$[Pa]$
$\mathbf{q}$	: heat flux	$[Wm^{-2}]$
Q_w	: heat production	$[J]$
r_o	: distance to the source point	$[m]$
R	: specific gas constant	$[JK^{-1}mol^{-1}]$
R_j	: radial function for infinite node j	
R_j^d	: radial function of order d for node j	
s	: entropy	$[Jkg^{-1}K^{-1}]$
S	: boundary	
S_i	: mapping functions for the interface Γ	
S_M	: Modal boundary	
S_s	: soft wall	
S_v	: vibrating wall	
t	: time	$[s]$
T	: Temperature	$[K]$
T_j	: circumferential function for infinite node j	
$\tilde{u}_n$	: normal displacement of a vibrating wall	$[m]$
$\mathbf{v}$	: fluid velocity	$[ms^{-1}]$
$\mathbf{v}_0$	: steady mean fluid velocity	$[ms^{-1}]$
$\mathbf{v}_\infty$	: fluid velocity at large distance from the source	$[ms^{-1}]$
$\mathbf{v}_a$	: acoustic velocity	$[ms^{-1}]$
$\tilde{\mathbf{v}}_a$	: amplitude of the harmonic acoustic velocity	$[ms^{-1}]$
$\mathscr{V}$	: the Sobolev space $W^{1,2} = H^1 = \{f : f, \nabla f \in L^2\}$	
V_{jl}	: l^{th} local approximation function of node j	
$\tilde{w}_n$	: normal velocity of a vibrating wall	$[ms^{-1}]$
W_j	: weight function of node j	
W_j^I	: infinite weight function of the infinite node j	
$W_{M,nm}$	: modal weight function of the angular and radial mode (m, n)	

Operators

∇	: gradient operator
$\nabla\cdot$	: divergence operator
$\nabla\times$	: curl operator
Δ	: Laplacian operator
$\frac{D}{Dt}$	: Total time derivative
:	: the double dot product of two tensors
$\langle\ \rangle$	: time average
$\Re$	: Real part

Contents

3

Axisymmetric formulation: Verification tests

This chapter compares numerical results obtained with the Mapped Infinite Partition of Unity Method to analytical solutions or numerical results computed with the commercial code ACTRAN^{TM}. The aim is to verify the axisymmetric formulation. Various applications are illustrated with the aim to tackle all the potentialities of the model: closed or unbounded domains, different boundary conditions, no-flow or convected simulations, topology of the elements, enrichment functions and infinite shape function parameters.

The performances of the axisymmetric method with respect to formulation parameters are evaluated in chapter 5 in terms of accuracy, computational time and frequency range.

3.1 Duct propagation

In this section we consider noise propagation in an infinite duct. The simulations are performed by considering a finite section of the infinite duct and by prescribing modal boundary conditions at both ends (fig. 3.1). As explained in section 2.9.2, the modal condition allows us to prescribe the amplitude of the incident acoustic modes. It also permits to avoid reflections of waves coming from the computational domain on the modal surface. We consider one incident mode prescribed at the left modal boundary condition. We distinguish the left modal boundary condition to the right one by calling the right condition: transmitted boundary condition as we do not prescribe incident mode from the right.

We simulate duct propagation within a finite duct (figure 3.1), bounded by modal boundary conditions. This duct can be considered as a 'closed domain' as no infinite elements have to be used. We use this application to verify our discretization method and assess its performances (in 5.1) in 'inner regions'.

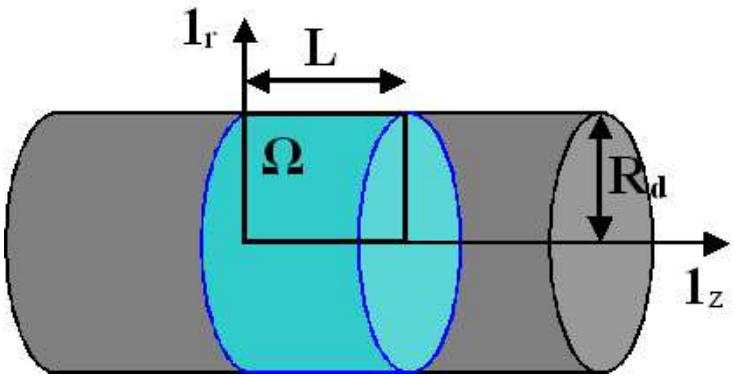

Fig. 3.1. Geometry of the duct: infinite duct in grey, finite duct in blue and the axisymmetric computational domain Ω given by the black rectangular domain.

Several simulations are performed to analyse different aspects and to illustrate the propagation:

- Propagation of a propagating mode in a hard walled duct;
- Propagation of an evanescent mode in a hard walled duct;
- Propagation of a propagating mode in a partially lined duct (i.e.: acoustic treatment of finite length applied on the inner duct walls);
- Convected propagation in a uniform mean flow in a hard walled duct;
- Convected propagation in a uniform mean flow in a lined duct.

As mentioned, the computations in this chapter are performed with an axisymmetric model. The geometry of the whole duct is obtained by rotating the computational domain around the axisymmetry axis and the pressure outside the computational plane is obtained by multiplying the computed pressure by the factor $e^{-im\theta}$, where m is the azimuthal mode and θ the azimuthal angle ($\theta = 0$ for the computational plane). The computational region consists in a rectangular domain (figure 3.1). The modal boundary is located between $(z, r) = (0, 0)$ and $(0, R_d)$, where R_d is the radius of the duct. The transmitted boundary is between $(L, 0)$ and (L, R_d), with L the length of the computational region. The wall of the duct is located at $r = R_d$. The radius has been chosen to be equal to $R_d = 0.5m$ and the length $L = 1m$. A typical mesh of the computational region and the modal boundaries are shown in figure 3.2. This mesh has been chosen so that there are more than 10 elements per wavelength. The computed results may then be assumed to be accurate.

3.1.1 Propagating mode in a hard walled duct

The first application corresponds to the propagation of a wave at 800Hz ($kR_d = 7.39$), of the second radial mode ($n = 2$) of the first azimuthal order ($m = 1$). The wall of the

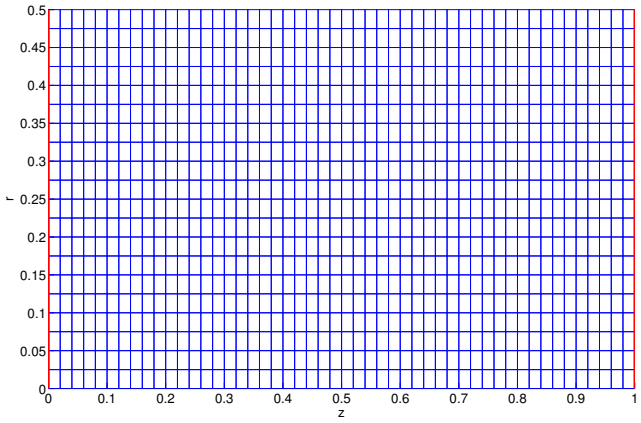

Fig. 3.2. Computational domain meshed with 50 elements in the axial direction and 20 in the radial one. The modal and transmitted boundary conditions are illustrated in red.

duct is chosen to be without acoustic treatment (hard wall). We assume there is no mean flow in the duct. The mesh generated for the simulation is composed of 50 elements in the axial direction and 20 in the radial one and the simulation is performed for a constant enrichment: $V_{j1} = \{1\}$. The aim is to verify the method, the performances are analysed further.

The MIPUM 0[1] computed results and the analytical solution are shown in figure 3.3 and figure 3.4, respectively. The analytical solution is given at section 2.6.1, by considering the unique mode $(m = 1, n = 2)$ at 800Hz. Figure 3.5(a) corresponds to representation of the discrete L^2 norm (equation 3.1) and figure 3.5(b) illustrates the relative discrete L^2 norm (equation 3.2). One may conclude that both solutions are close as the relative error keeps under a level of 5%. Note that the differences grow with the axial direction so with the wave propagation. This is due to the dispersion of the numerical scheme. The relative L^2 norm is a good indicator of the accuracy of the computed solution. But care has to be taken with this indicator, especially when the absolute part of the analytical solution is close to zero as it is the case in this application for $r = 0m$ and r close to $0.35m$.

$$\left|\tilde{p}^h\left(\mathbf{x}_j\right) - \tilde{p}_{an}\left(\mathbf{x}_j\right)\right| \tag{3.1}$$

$$100\left|\tilde{p}^h\left(\mathbf{x}_j\right) - \tilde{p}_{an}\left(\mathbf{x}_j\right)\right| / \left|\tilde{p}_{an}\left(\mathbf{x}_j\right)\right| \tag{3.2}$$

[1] MIPUM $i-j-k$ corresponds to the Mapped Infinite Partition of Unity Method with an enrichment of polynomial order i. Indices j and k correspond to the infinite radial and circumferential order respectively. They are omitted in the case of inner region (no infinite elements)

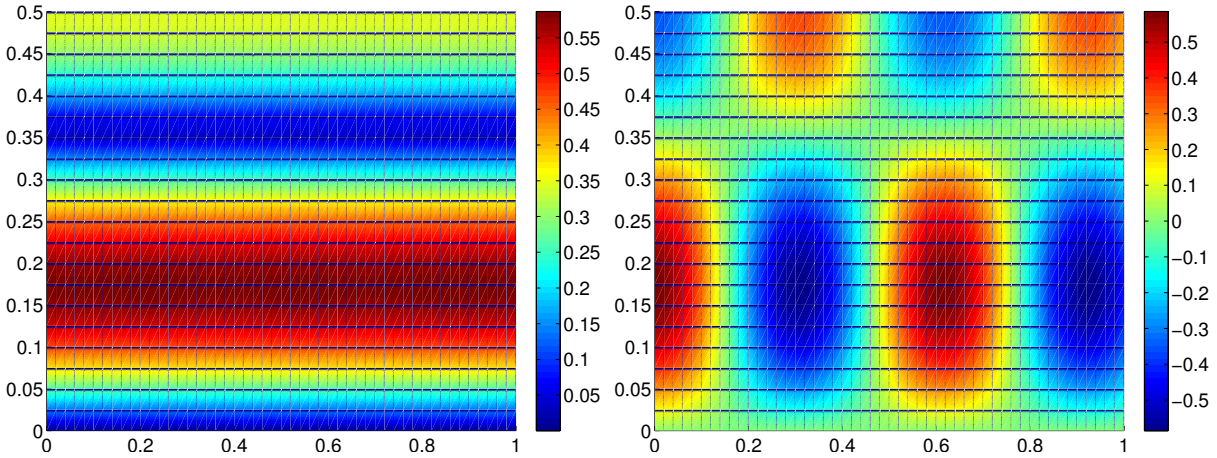

(a) (b)

Fig. 3.3. MIPUM 0 computed results for the propagation at 800 Hz of the second mode of the first azimuthal order in a hard walled duct: (a) Absolute part of the acoustic pressure (b) Real part of the acoustic pressure.

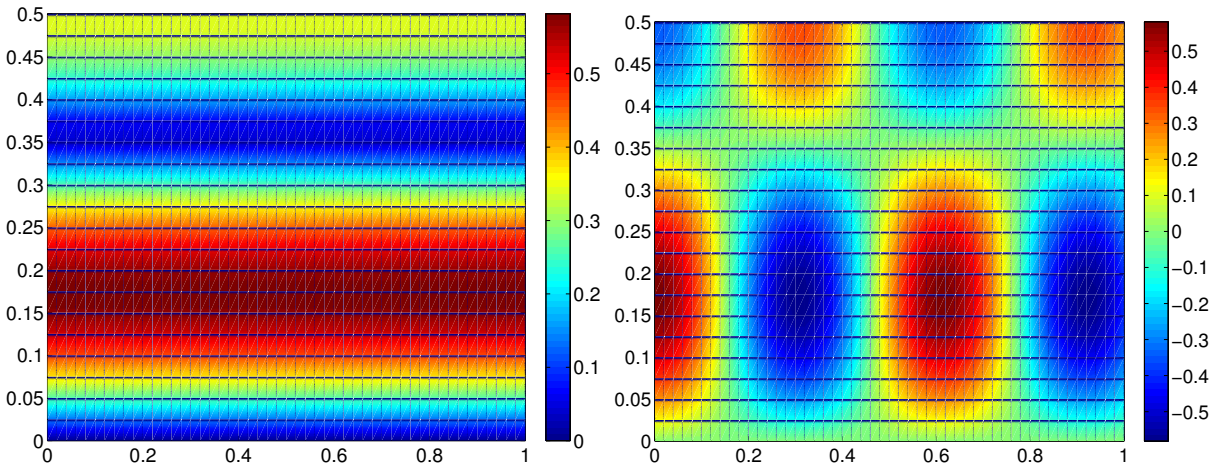

(a) (b)

Fig. 3.4. Analytical results for the propagation at 800 Hz of the second mode of the first azimuthal order in a hard walled duct: (a) Absolute part of the acoustic pressure (b) Real part of the acoustic pressure.

3.1.2 Evanescent mode in a hard walled duct

This section illustrates the acoustic pressure distribution in the case of the prescription of an evanescent mode. MIPUM 0 numerical result is compared to the analytical solution as it has been done for the previous application. This application is quite identical to the previous one, except for the radial mode which is prescribed. In this case, we choose to prescribe the fourth radial mode of the first azimuthal test case $n = 4$ & $m = 1$. The mesh generated for the simulation is composed of 50 elements in the axial direction and 20 in the radial one (as for the previous application). The simulation is performed for a constant enrichment: $V_{j1} = \{1\}$.

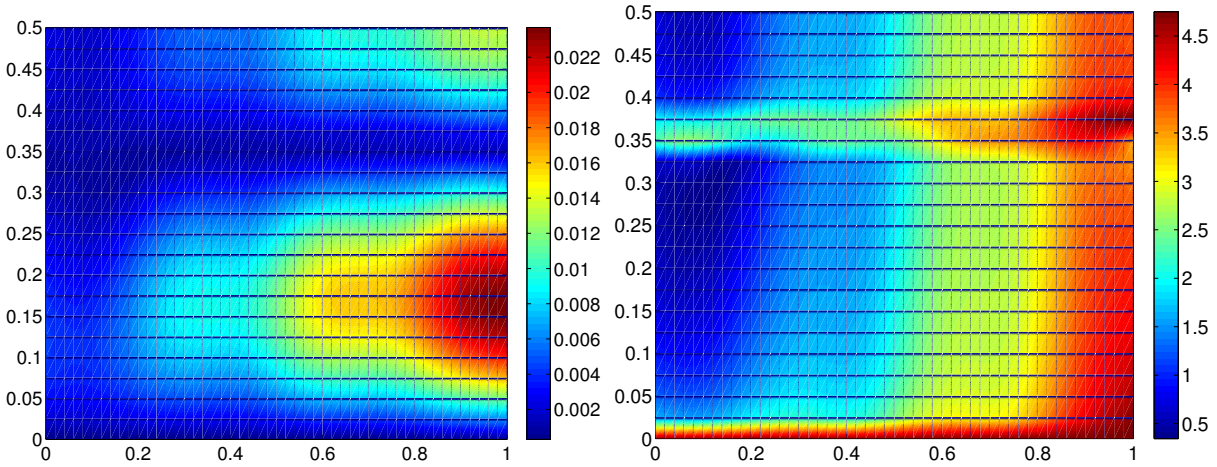

(a) (b)

Fig. 3.5. Propagation at 800 Hz of the second mode of the first azimuthal order in a hard walled duct: MIPUM 0 (a) Discrete L^2 norm (b) Relative discrete L^2 norm [%].

MIPUM 0 computed absolute and real part of the pressure are shown in figure 3.6. Figure 3.7 illustrates analytical values where the analytical solution is given at section 2.6.1, by considering the unique mode $(m = 1, n = 4)$ at 800 Hz. The comparison of the analytical and computed results are shown figure 3.8. The relative discrete L^2 norm is not shown here as a large part of the analytical solution is close to zero. This leads to high values of relative discrete L^2 norm while the approximation is accurate. In this case, the relative discrete L^2 norm is not a good indicator of the accuracy. We can conclude that the method is suitable to analyse wave propagation in hard walled ducts and that we are able to simulate as well propagating as evanescent duct modes.

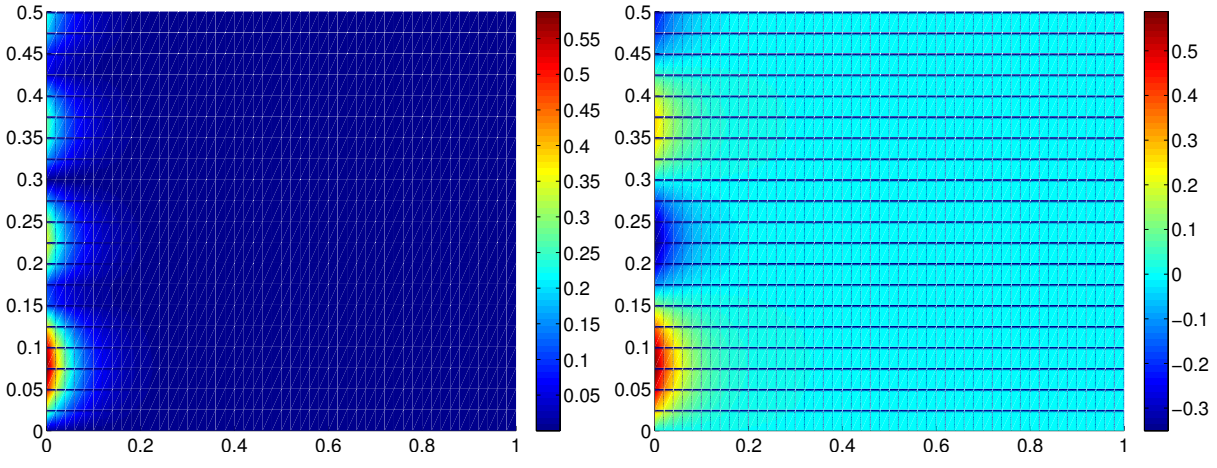

(a) (b)

Fig. 3.6. MIPUM 0 computed results for the propagation at 800 Hz of the fourth mode of the first azimuthal order in a hard walled duct: (a) Absolute part of the acoustic pressure (b) Real part of the acoustic pressure.

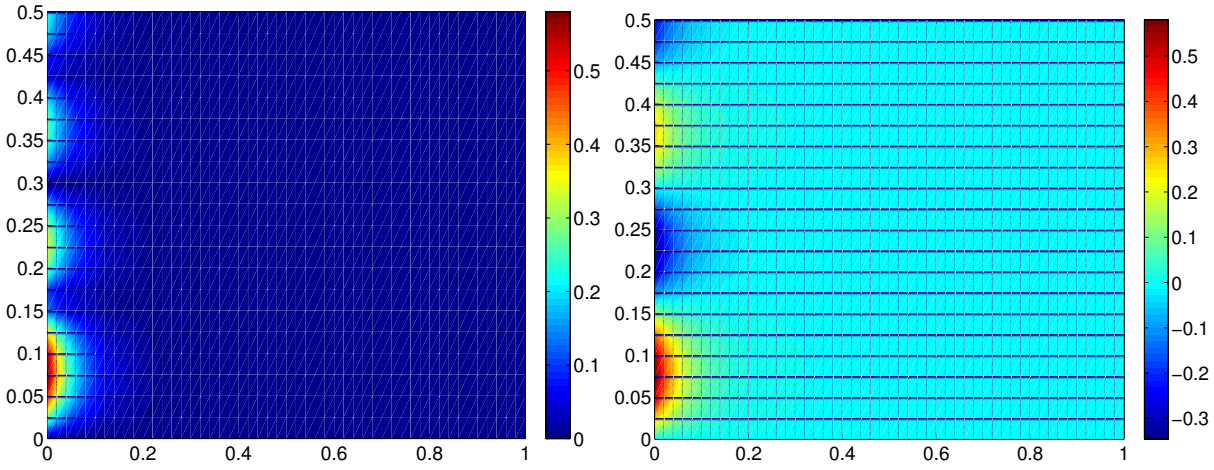

(a) (b)

Fig. 3.7. Analytical results for the propagation at 800 Hz of the fourth mode of the first azimuthal order in a hard walled duct: (a) Absolute part of the acoustic pressure (b) Real part of the acoustic pressure.

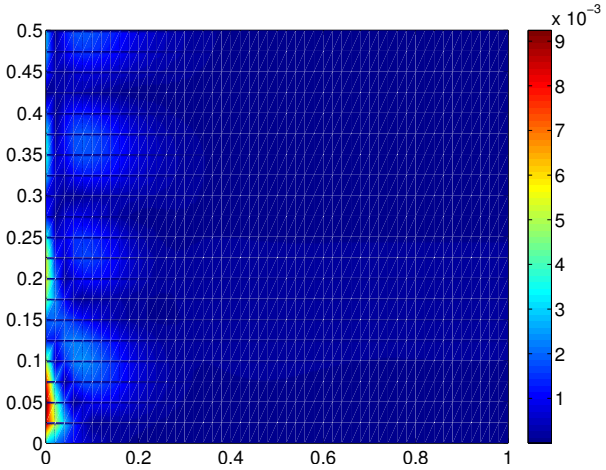

Fig. 3.8. Propagation at 800 Hz of the fourth mode of the first azimuthal order in a hard walled duct: MIPUM 0 discrete L^2 norm.

3.1.3 Propagating mode in a lined duct

We consider the same duct but we place a soft wall of finite length inside the duct. The liner is uniform in the azimuthal direction, it is not segmented (there are no splices). It is located between $(0.14m, R_d)$ and $(0.42m, R_d)$. The acoustic properties of the liner are given by the normal admittance: $A_n = 0.001 + 0.002i\,[m^3N^{-1}s^{-1}kg^{-1}]$.

We prescribe an incident mode through a modal boundary condition. The prescribed mode is the same as prescribed for the first application: excitation frequency 800 Hz,

second radial order ($n = 2$) and first azimuthal order ($m = 1$). This choice has been done to illustrate the effect of the liner. The first application shows the propagation in a hard walled duct while this section illustrates the same conditions except for the presence of an acoustic treatment.

MIPUM 0 numerical results are compared to the simulation obtained with the commercial code ACTRAN^{TM}. Both meshes are identical (50 elements in the axial direction and 20 in the radial one) and both simulations are carried out with quadrangles linear Finite Elements (note that in our case it is equivalent to a constant enrichment ($V_{j1} = \{1\}$) as demonstrated in section 2.5).

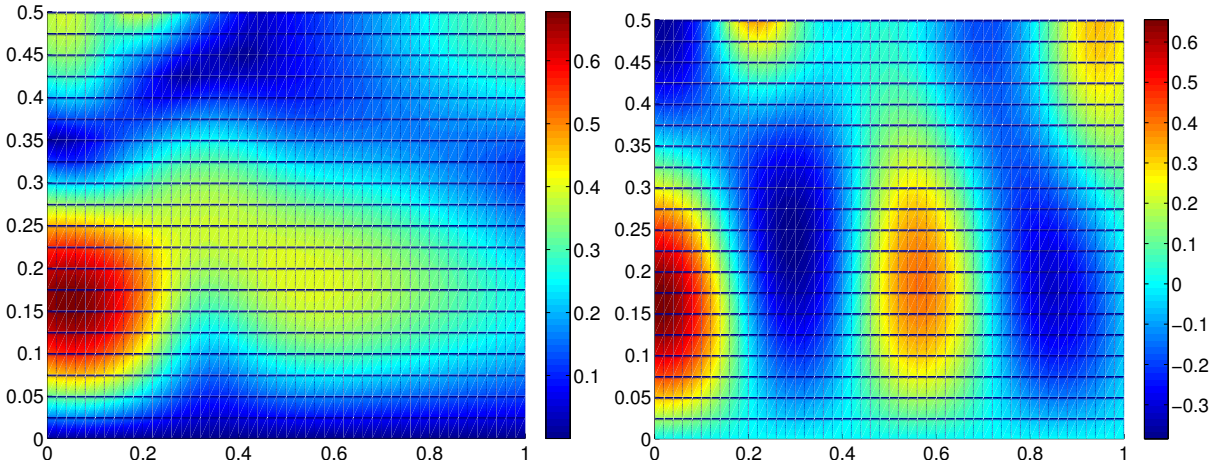

(a) (b)

Fig. 3.9. MIPUM 0 computed results for the propagation at 800 Hz of the second mode of the first azimuthal order in a partially lined duct: (a) Absolute part of the acoustic pressure (b) Real part of the acoustic pressure.

Both simulations (MIPUM 0 in figure 3.9 and linear finite elements (ACTRAN^{TM}) in figure 3.10) give the same results and show the decay of the amplitude of the initial incident wave. Also note that the outgoing noise at the end of the duct is no longer the incident mode. The presence of the liner scatters the mode in a combination of radial order modes n with the same azimuthal order m. This last remark stands only for liner without splices. In the case of splices in the azimuthal direction (frequent in industrial applications as it facilitates the manufacture and installation) the wave will also be scattered in the azimuthal direction.

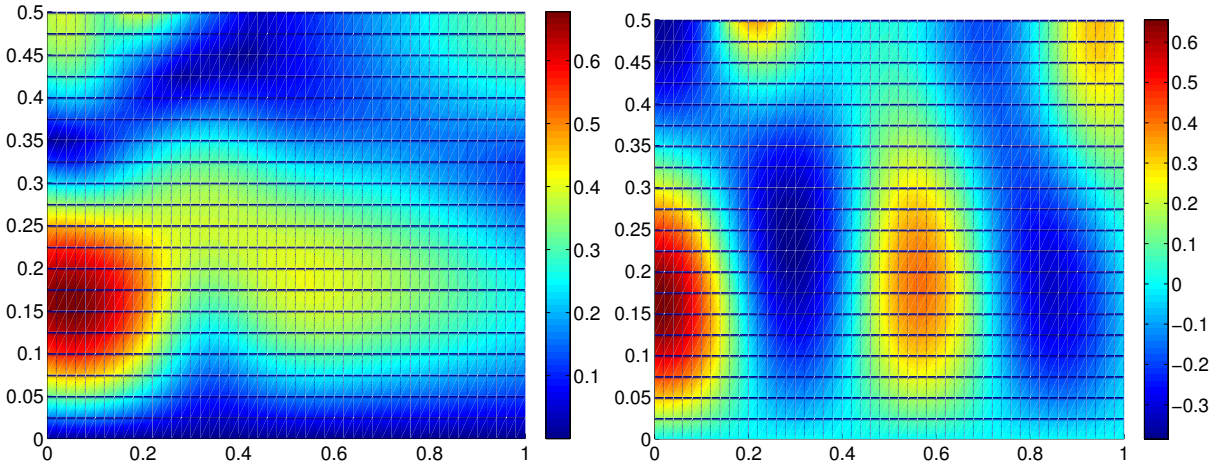

(a) (b)

Fig. 3.10. Computed results with ACTRAN^{TM} for the propagation at 800 Hz of the second mode of the first azimuthal order in a partially lined duct: (a) Absolute part of the acoustic pressure (b) Real part of the acoustic pressure.

3.1.4 Convected propagation in a hard walled duct

This section illustrates wave propagation in the presence of flow. We keep the same configuration of the first application: propagating wave at 800 Hz in the axial direction, second radial order $n = 2$ and first azimuthal order $m = 1$. The difference consists in considering an axial mean flow $\mathbf{v}_0 = -100m/s\mathbf{1}_z$. Note that the negative value indicates that the flow goes in the opposite direction than the wave.

The flow modifies the distribution of the pressure[2]. In this case (upstream propagation), we observe a shortening of the wavelength in the axial direction while the radial wavelength has not been modified. The generation of the mesh for convected propagation require to take into account the effect of the flow.

Figure 3.11 shows MIPUM 0 computed results and figure 3.12 illustrates the discrete L^2 norms with the analytical solution calculated as explained in section 2.6.1. We observe as expected that the effect of upstream flows (shortening of the axial wavelength by a factor close to 0.7) decreases the accuracy of the approximation compared to the 'no-flow' case with the same mesh (figure 3.5). The number of elements per wavelength has been divided by a factor 1.4: from 30 elements per wavelength for the no flow application to 20 elements per wavelength for the convected case. To increase the accuracy, a finer mesh should be generated or a higher enrichment order has to be used.

[2] The effect of uniform mean flow is illustrated in appendix 10.4 for free propagation of a plane wave in a two-dimensional domain.

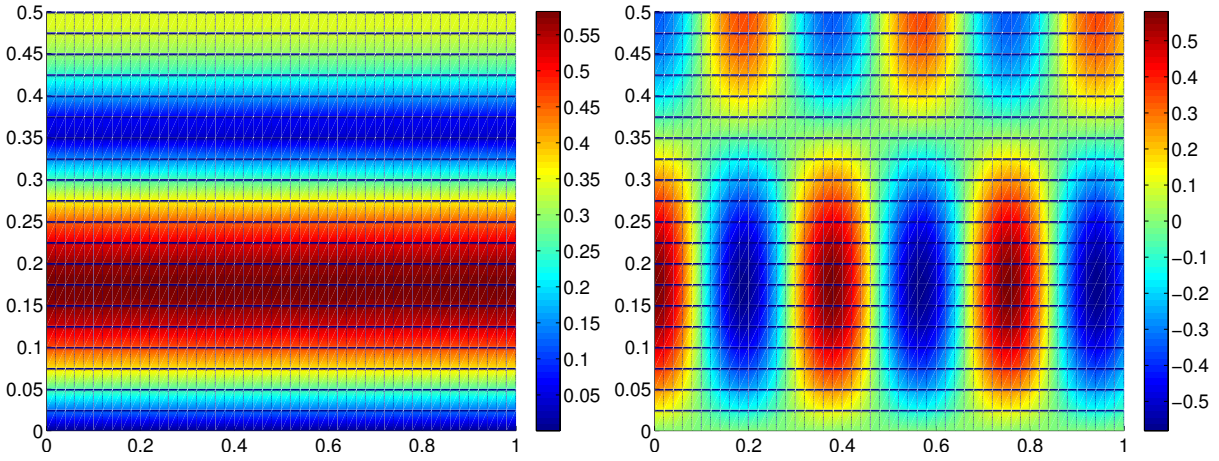

(a) (b)

Fig. 3.11. MIPUM 0 computed results for the convected ($\mathbf{v}_0 = -100m/s\mathbf{1}_z$) propagation at 800 Hz of the second mode of the first azimuthal order in a hard walled duct: (a) Absolute part of the acoustic pressure (b) Real part of the acoustic pressure.

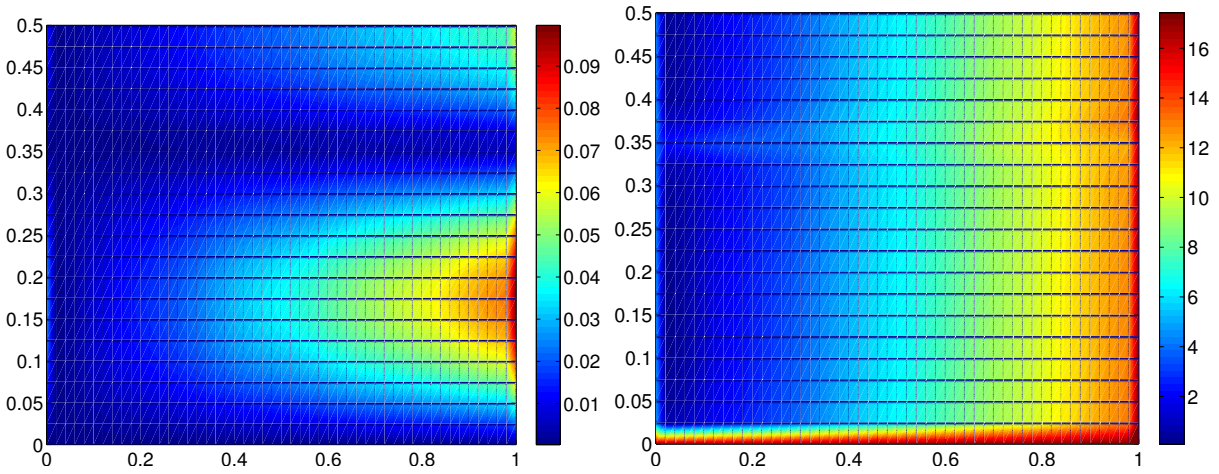

(a) (b)

Fig. 3.12. Convected ($\mathbf{v}_0 = -100m/s\mathbf{1}_z$) propagation at 800 Hz of the second mode of the first azimuthal order in a hard walled duct: MIPUM 0 (a) Discrete L^2 norm (b) Relative discrete L^2 norm [%].

3.1.5 Convected propagation in a lined duct

This last application concerning duct propagation considers all the aspects together (i.e. convected propagation in a lined duct). The wave which propagates with an excitation frequency of 800 Hz in the duct is given by the mode $(m = 1, n = 2)$. The mean flow is uniform in the duct: $\mathbf{v}_0 = -100m/s\mathbf{1}_z$. The liner $(An = 0.001 + 0.002i)$ is located between the positions $(0.14m, R_d)$ and $(0.42m, R_d)$.

MIPUM 0 numerical results (figure 3.13) are compared to ACTRAN^{TM} simulations (figure 3.14) as it has been done for the non convected case.

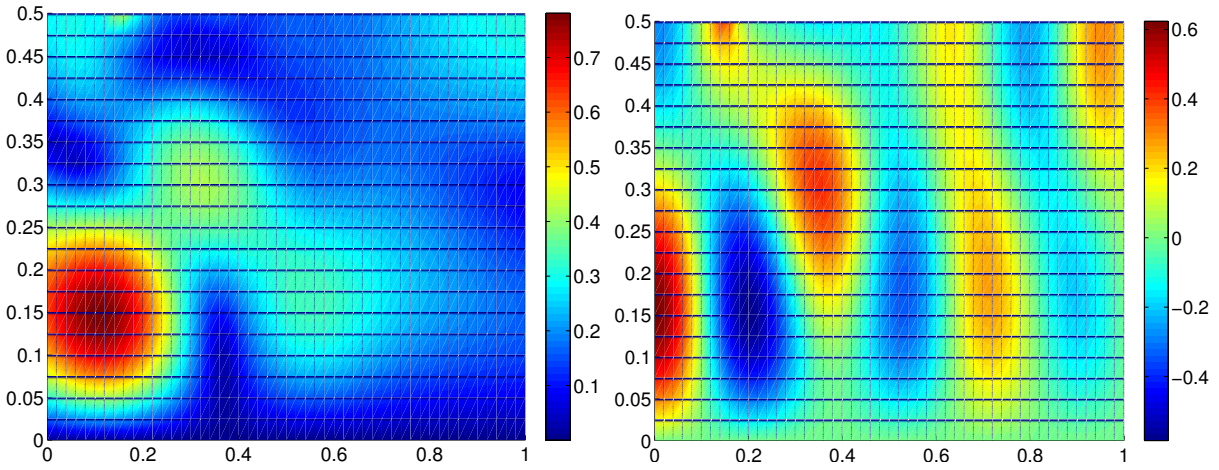

(a) (b)

Fig. 3.13. MIPUM 0 computed results for the convected ($\mathbf{v}_0 = -100m/s\mathbf{1}_z$) propagation at 800 Hz of the second mode of the first azimuthal order in a lined duct: (a) Absolute part of the acoustic pressure (b) Real part of the acoustic pressure.

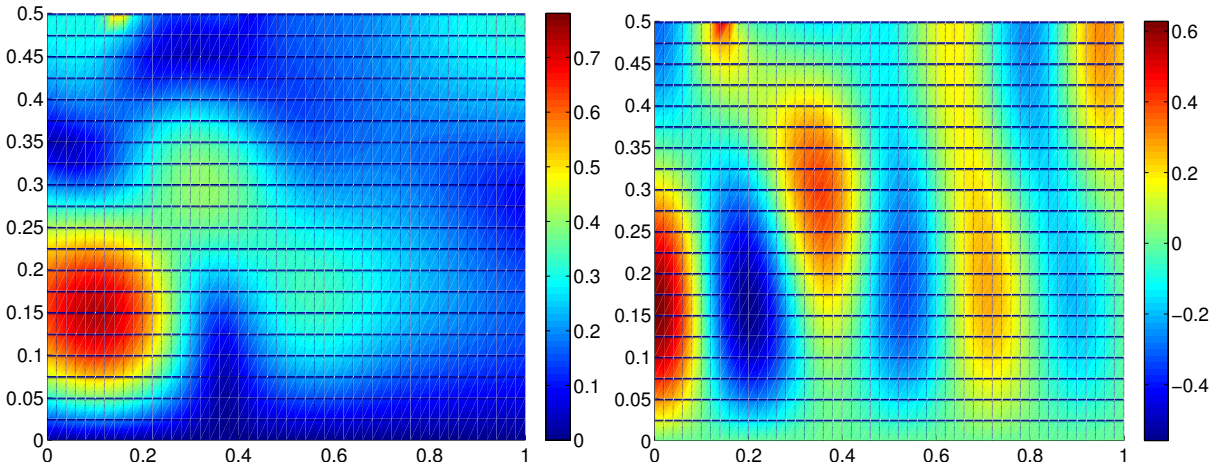

(a) (b)

Fig. 3.14. ACTRAN^{TM} results for the convected ($\mathbf{v}_0 = -100m/s\mathbf{1}_z$) propagation at 800 Hz of the second mode of the first azimuthal order in a lined duct: (a) Absolute part of the acoustic pressure (b) Real part of the acoustic pressure.

This completes the verification of the axisymmetric model in the case of bounded applications. We analysed modal and transmitted boundary conditions, admittance boundary condition and the effect of uniform mean flow on the propagation.

3.2 Propagation in a non-uniform duct

We illustrate simulations for a convected propagation by considering a non-uniform mean flow. This is performed by considering the propagation in a duct with non-uniform cross section. The geometry is inspired from the inlet of a turbofan (equations 3.3). This geometry has been analysed previously by Rienstra and Eversmann [36] in comparing multiple scale and Finite Element solutions and by Gamallo and Astley [17] in comparing the Partition of Unity Finite Element Method with a set of plane waves as solutions and the Finite Element Method.

$$
\begin{aligned}
R_1(z) &= max\left[0,\ 0.64212 - \sqrt{0.04777 + 0.98234 z'^2}\right] \\
R_2(z) &= 1 - 0.18453 z'^2 + 0.10158 \frac{e^{-11(1-x')} - e^{-11}}{1 - e^{-11}}
\end{aligned}
\tag{3.3}
$$

with R_1 and R_2 being the radii of the spinner and the outer wall respectively, $z' = z/L$ and $L = 1.86393m$. Note that computational region is composed of the geometry of the inlet terminated by a uniform circular duct of $1m$ long. The aim is to move the terminal plane far from mean flow non-uniformities so that we can assume the mean flow to be uniform at the terminal plane. The mean flow mach number is illustrated in figure 3.15. The mean flow has been computed by the software ACTRAN^{TM} by prescribing the normal velocity on each duct termination. We considered the flow to be irrotational and incompressible. Note that the mean flow is computed on the acoustic mesh of each simulations.

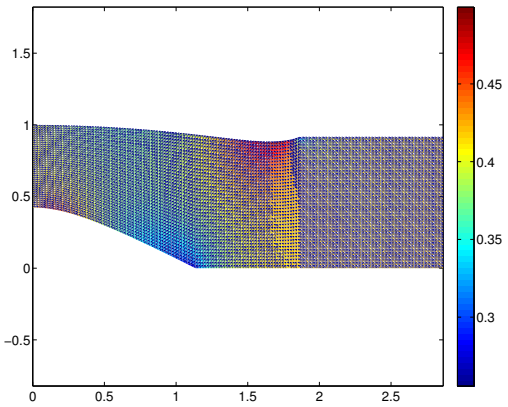

Fig. 3.15. Mean flow mach number.

We analyse the propagation of a plane wave at 1600 Hz ($ka = 29.57$ for $a = 1m$). This is prescribed by a modal boundary condition on the source plane and a transmitted boundary condition on the terminal plane.

We compare computational results obtained with the Partition of Unity Method to the linear Finite Element Method (ACTRAN^{TM}). The Partition of Unity simulation (fig. 3.16(a)) is based on a mesh with 200 Q4 elements in the axial direction and 40 in the radial one. The enrichment functions are polynomials of second order: $V_{jl} = \left\{1, (z-z_0), (r-r_0), (z-z_0)^2, (r-r_0)^2\right\}$. This leads to 41226 degrees of freedom. The ACTRAN^{TM} solution (figure 3.16(b)) is based on a finer mesh of 600 Q4 elements in the axial direction and 70 in the radial one but the number of unknowns is quite the same: 42692 degrees of freedom. This corresponds to approximately 25 elements per wavelength (an overview of the meshes generated is shown figure 3.17). Both simulations are very close, showing that the enrichment functions are well implemented. This verifies the model for non-uniform mean flows.

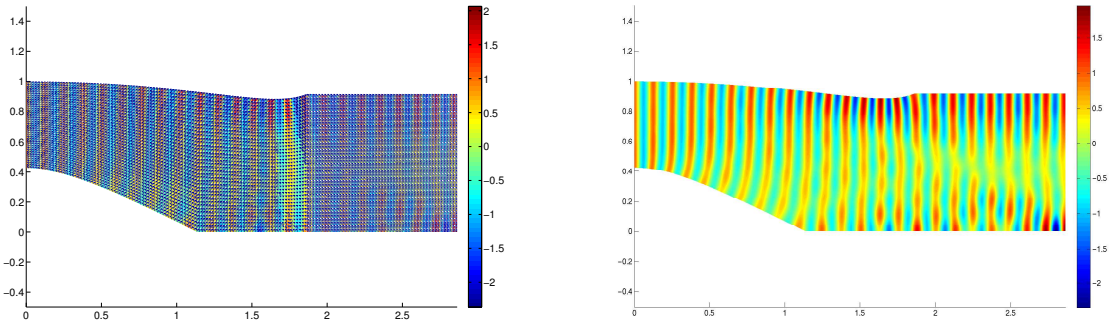

(a) (b)

Fig. 3.16. Computed results (real part of the pressure) for plane wave propagation at $1600Hz$ ($ka = 29.57$ for $a = 1m$): (a) Second order enrichment for the Partition of Unity Method (41226 dofs) (b) Linear Finite Element Method (42692 dofs).

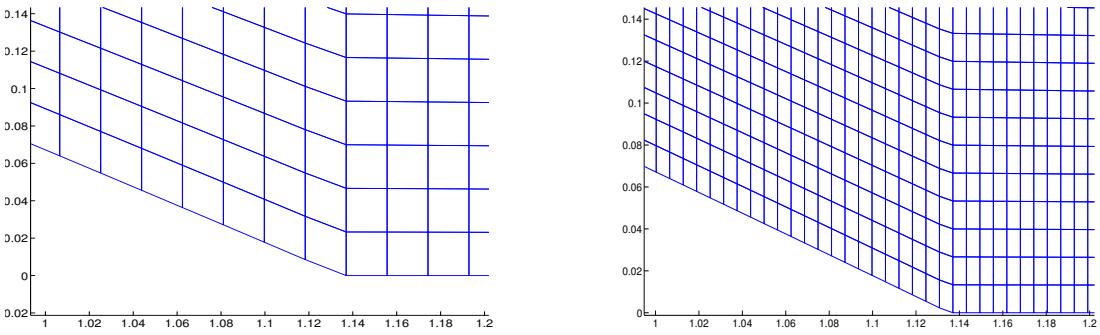

(a) (b)

Fig. 3.17. Mesh around the spinner: (a) mesh 200 $\times$ 40 (b) mesh 600 $\times$ 70.

3.3 Multipole radiation

This section analyses the properties of the Mapped Infinite Partition of Unity Method on the radiation of a multipole. We first verify the Mapped Infinite Partition of Unity Method by comparing the numerical solution to the analytical one. We then examine the parameters of the method and their effect on the accuracy (section 5.2).

Multipole radiation is simulated by prescribing acceleration on a vibrating sphere. The radius of the vibrating sphere is r_S and the interface Γ separating the infinite domain in an inner and an outer region is a sphere of radius r_Γ (figure 3.18). The inner region is meshed either by Q8 elements[3] while the outer region is partitioned with infinite elements of radial order m_0 and the circumferential polynomial is of order b_0.

The analytical solution [30] for the multipole of order N and azimuthal order m is given by equation (3.4) where P_N^m denotes the associated Legendre polynomial which reduces to Legendre polynomial of order N in case of $m = 0$, γ is the spherical polar angle, θ the azimuthal angle, r is the spherical polar radius and $h_N^{(2)}$ the spherical Bessel function of the second kind.

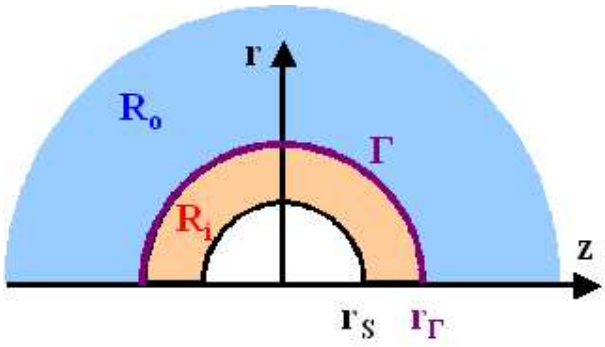

Fig. 3.18. Multipole: axisymmetric domain and geometry.

This work investigates multipole radiation with $m = 0$ and $N = 1$ or $N = 7$. This is generated by prescribing an acceleration on the vibrating sphere: $\bar{a}_n = a_0 \, P_N \left(cos \left(\gamma \right) \right)$.

$$\tilde{p}_{an} \left(\mathbf{x} \right) = \left(\frac{\rho_0 a_0}{k} \right) P_N^m \left(cos \left(\gamma \right) \right) \frac{h_N^{(2)} \left(kr \right)}{h_N^{(2)'} \left(kr_S \right)} e^{im\theta} \tag{3.4}$$

Figure 3.19 illustrates the distribution of the real part of the pressure of the dipole ($N = 1$). The excitation frequency is 1100Hz ($kr_S = 20.3$), $r_S = 1m$. The domain is infinite, but the pressure distribution has been represented between the vibrating sphere and the interface Γ, with $r_\Gamma = 3m$.

[3] Q8 elements are the elements described in the axisymmetric formulation 2.9.1 with 4 nodes and 4 mapping points. We also developed a Q4 element which is not detailed in this work but corresponds to a classical element with linear edges (no mapping points). The influence of the mapping is shown in section 5.2.

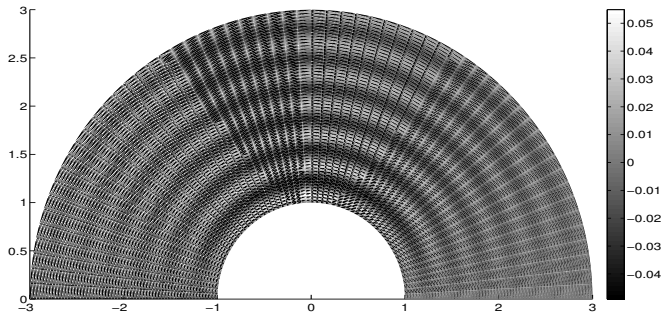

Fig. 3.19. Dipole radiation: real part of the computed pressure ($1100Hz, kr_S = 20.3$), $r_S = 1m$, $r_\Gamma = 3m$, number of elements in the radial direction: $n_r = 60$, and in the circumferential one: $n_\theta = 60$, radial order of infinite elements $m_0 = 2$, circumferential order of infinite elements $b_0 = 1$ and enrichment in the inner region $V_{j1} = \{1\}$: MIPUM 0 2 1.

Figure 3.20 illustrates the distribution of the real part of the computed pressure for the radiation of a multipole of order $N = 7$. The excitation frequency is 700Hz ($kr_S = 12.94$), $r_S = 1m$ and $r_\Gamma = 3m$. The computed results are obtained by using an inner mesh of 70 elements in the radial direction and 70 in the circumferential one. The inner enrichment is $V_{j1} = \{1\}$. 70 infinite elements are attached to the inner mesh. Each infinite element is of radial order $m_0 = 8$ and the circumferential one is $b_0 = 1$. The domain is infinite, but for practical reasons the real part of the pressure has been represented in the inner region and in an outer region bounded with $z \in [-4,\ 4]$ and $r \in [0,\ 4]$.

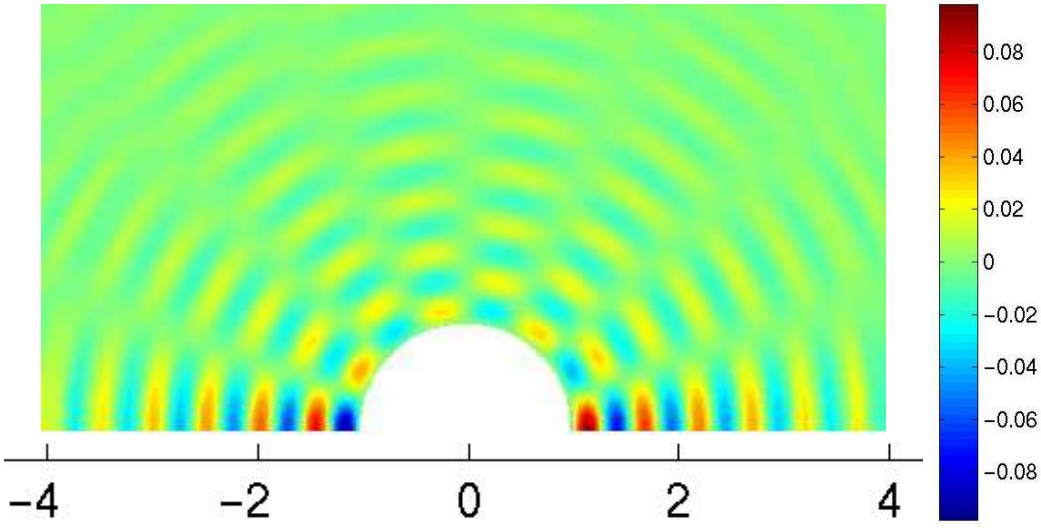

Fig. 3.20. Multipole ($N = 7$) radiation: real part of the MIPUM 0 2 1 computed pressure ($700Hz, kr_S = 12.94$), number of elements in the radial direction: $n_r = 70$, and in the circumferential one: $n_\theta = 70$.

The absolute part of the computed pressure is compared to the analytical one (figure 3.21). The region where the pressure is illustrated is given by the points satisfying: $\sqrt{z^2 + r^2} < 8m$.

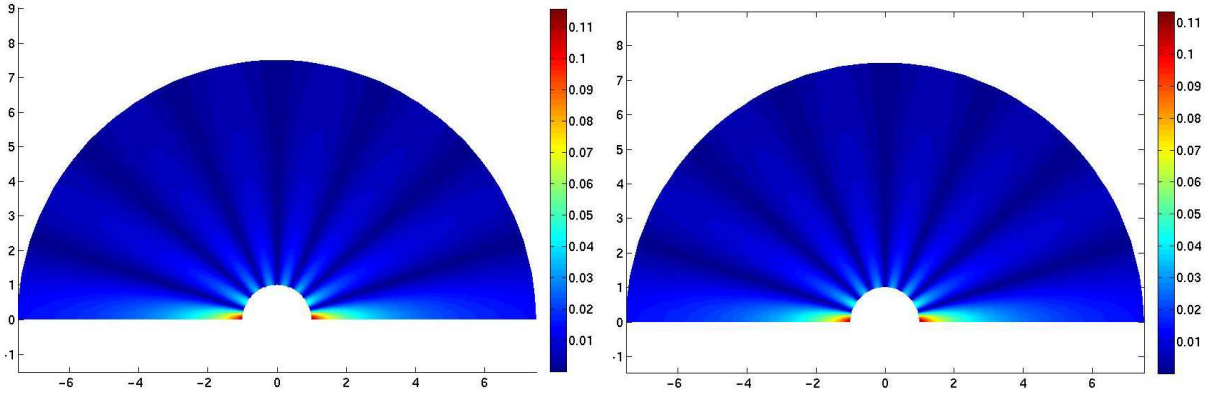

(a) (b)

Fig. 3.21. Multipole ($N = 7$) radiation: Absolute part of the MIPUM 0 2 1 computed (a) and analytic (b) pressure ($700Hz, kr_S = 12.94$), number of elements in the radial direction: $n_r = 70$, and in the circumferential one: $n_\theta = 70$.

Figure 3.22(a) represents the discrete L^2 norm $\left|\tilde{p}^h - \tilde{p}_{an}\right|$ and figure 3.22(b) illustrates the relative discrete L^2 norm: $100\left|\tilde{p}^h - \tilde{p}_{an}\right| / \left|\tilde{p}_{an}\right|$. We conclude that MIPUM 0 2 1 solution is accurate even if we note that the relative discrete L^2 norm reaches 20%. This is due to analytic values close to zero.

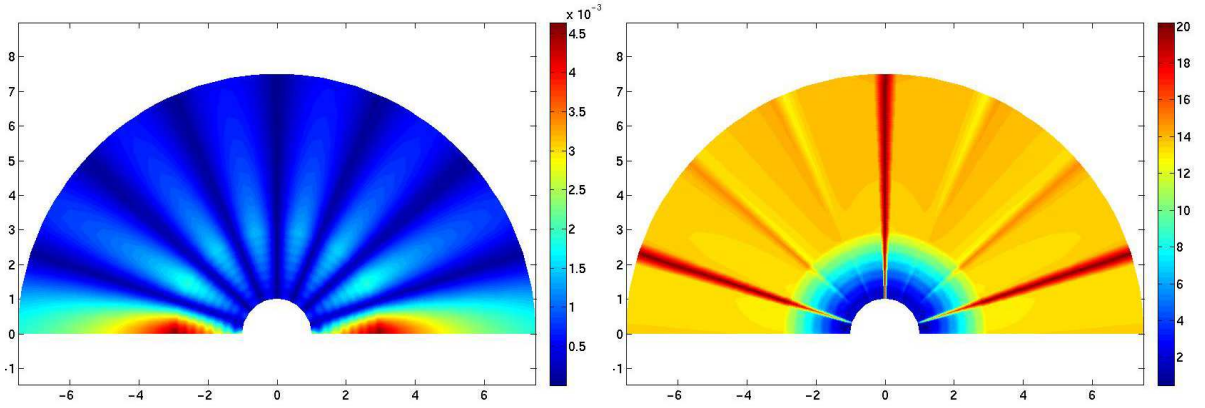

(a) (b)

Fig. 3.22. Multipole ($N = 7$) radiation: MIPUM 0 2 1 (a) Discrete L^2 norm (b) Relative discrete L^2 norm [%]: ($700Hz, kr_S = 12.94$), number of elements in the radial direction: $n_r = 70$, and in the circumferential one: $n_\theta = 70$.

3.4 Rigid piston radiation

This section does not bring a lot of new indications compared to the previous case of multipole radiation but it confirms what has been said. It illustrates the simulation of the radiation of a rigid piston in a non-convected semi-infinite region (figure 2.16).

We analyse the radiation of a piston of radius $r_p = 0.5m$ at 500 Hz. The vibration is prescribed by an acceleration boundary condition ($\tilde{a}_n = 1m/s^2$). The inner region is limited by the square $(0,0) \times (1,1)$. It is meshed with Q4 elements.

Figure 3.23 illustrates the radiation by the absolute and the real part of the pressure. The simulation has been computed with the constant enrichment functions $\{1\}$. The mesh is composed of 36 elements in the radial direction and 19 in the axial one. The infinite radial order is equal to $m_0 = 4$ (it has been verified for this mesh that an increase in radial order does not improve the accuracy).

The numerical results are compared to the analytical solution in figure3.24. The analytical solution is obtained by Rayleigh integrals. The piston S_p is considered as a continuous distribution of monopoles [30, 74, 75, 76]. The analytical solution at a point $\mathbf{x}_Q = (z_Q, r_Q)$ is given by:

$$\tilde{p}_{an}(\mathbf{x}_Q) = \frac{-\rho_0 \tilde{a}_n}{2\pi} \int\int_{S_p} \frac{e^{-ikR}}{R} dS_p$$
$$R = \sqrt{\left(z_Q^2 + r_Q^2\right) + r^2 - 2 r_Q r cos(\theta)} \tag{3.5}$$

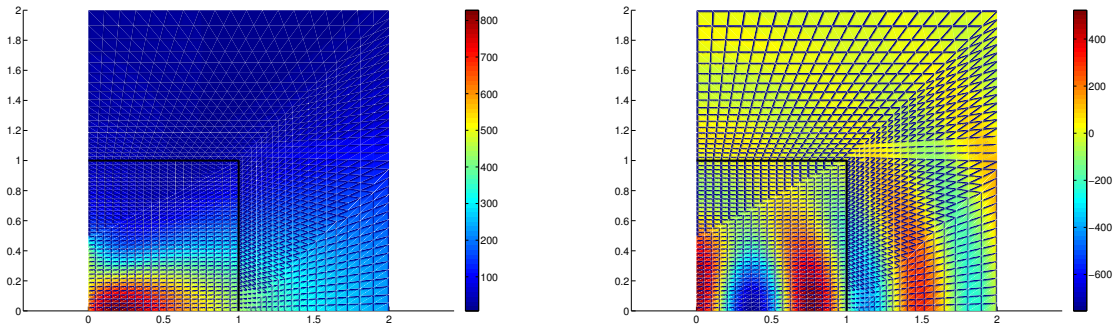

(a) (b)

Fig. 3.23. MIPUM 0-4-1 computed results for the radiation of a rigid piston at 500 Hz. The black line represents the interface Γ separating the inner and outer region. (a) Absolute part of the acoustic pressure (b) Real part of the acoustic pressure.

Note that the discrete L^2 errors in figure 3.24 are equal to zero at the piston. This has been prescribed manually.

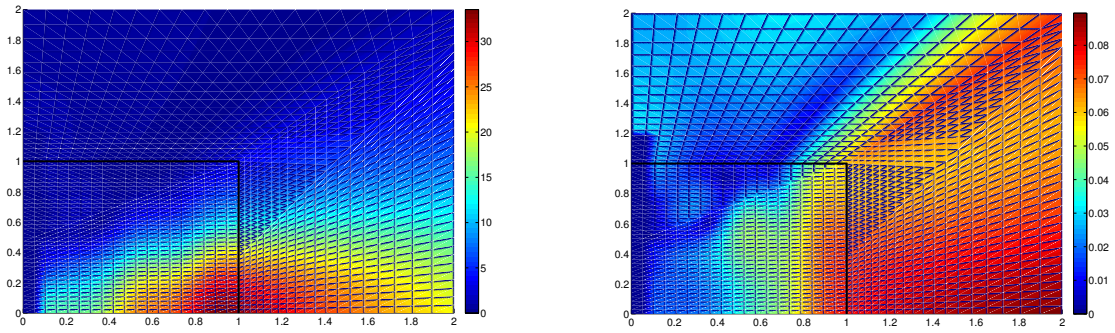

(a) (b)

Fig. 3.24. MIPUM 0-4-1 computed results for the radiation of a rigid piston in an infinite domain at 500Hz: (a) Discrete L^2 norm (b) Relative discrete L^2 norm.

This analysis confirms that the formulation is appropriate to simulate vibrating walls in infinite domains. This also illustrates that the shape of the interface Γ does not necessarily be a circle.

3.5 Radiation of an infinitesimal cylinder within a uniform mean flow

This section illustrates the Mapped Infinite Partition of Unity Method in the case of convected radiation. The application analysed is the radiation of an infinitesimal cylinder surrounded by a uniform mean flow along the axial direction $\mathbf{v}_0 = v_0 \mathbf{1}z$ (mach number M). The cylinder is of length $L = 0.5m$ and has a radius which tends to zero ($a \approx 0$). As the radius is infinitesimal, we assume that the distribution of the flow is not perturbed by the presence of the cylinder. This application has been previously analysed by Astley [77].

We prescribe a traveling structural wave (of wavenumber k_s) on the cylinder by giving the normal displacement:

$$u_n = u_0 e^{i\omega t - ik_s z} \tag{3.6}$$

This leads to prescribe on the cylinder:

$$\frac{\partial \tilde{\phi}_a}{\partial r}|_{r=a} = i\omega u_0 \left(1 + M\frac{k_s}{k} e^{ik_s z}\right) \tag{3.7}$$

The analytical solution is derived by considering the cylinder to be a distribution of monopole sources and by integrating the contributions on the cylinder ($\alpha = \omega a u_0 = 1$).

$$\tilde{\phi}_{an}(z,r) = \frac{i\alpha}{2}\left(1 - M\frac{k_s}{k}\right)\int_{-L/2}^{L/2}\frac{1}{R'}e^{(-ik_s z' - ik\Psi)}dz'$$
$$R' = \sqrt{(z-z')^2 + (1-M^2)\,r^2}$$
$$\Psi = \frac{M(z-z') + R'}{1-M^2} \tag{3.8}$$

The mesh used for the computation is shown in figure 3.25. The inner region is determined by the half circle: $\sqrt{z^2+r^2} < 1m$ and $r \geq 0m$. The mesh is generated by giving the number of mapped Q8 elements along the cylinder (n_p) and the number of elements in the radial direction (n_r). Note that the number of elements along the interface (hence the number of infinite elements) equals the number of elements along the piston increased by two ($n_p + 2$).

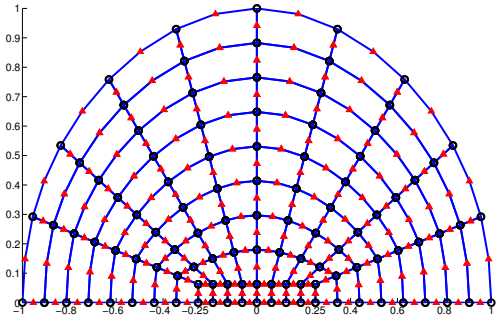

Fig. 3.25. Infinitesimal cylinder radiation: Mesh in the inner region ($n_p = 8, n_r = 8$). Elements are in blue, nodes are black circles and mapping points are red triangles. The cylinder is on the range $[-0.25, 0.25]$.

Figure 3.26 illustrates the distribution of the pressure in the inner and the outer region with a uniform mean flow: $\mathbf{v}_0 = -85m/s\ \mathbf{1}z$. The interface Γ is represented by the black line. The mesh is composed of $n_p = 30$ elements along the piston and $n_r = 30$ in the radial direction. The structural and acoustic wavenumbers are equal: $k_s = k = 9.24\ m^{-1}$ ($f = 500Hz$). The inner enrichment is the constant one: $V_{j1} = 1$. The infinite radial order is $m_0 = 4$ and the circumferential one: $b_0 = 1$.

The performances of Mapped Infinite Partition of Unity Method are analysed by comparing the computed and analytic pressures along the interface Γ for three enrichments (the circumferential enrichment is $b_0 = 1$ for the constant enrichment and $b_0 = 2$ for other enrichments):

- constant function with $n_p = 30$, $n_r = 30$ (1151 *dofs*) in figure 3.27,
- second order functions with $n_p = 12$, $n_r = 12$ (1120 *dofs*) in figure 3.28 and

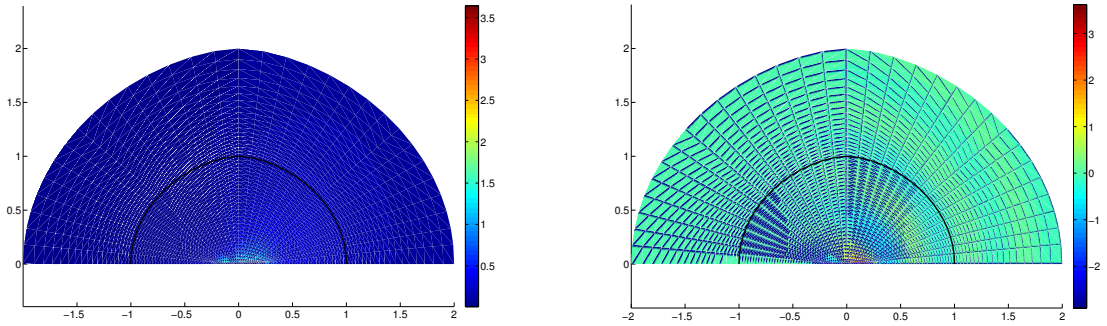

(a) (b)

Fig. 3.26. Computed results for the infinitesimal cylinder radiation at 500 Hz with a uniform mean flow $\mathbf{v}_0 = -85m/s\ \mathbf{1}z$: (a) Absolute part of the acoustic pressure (b) Real part of the acoustic pressure

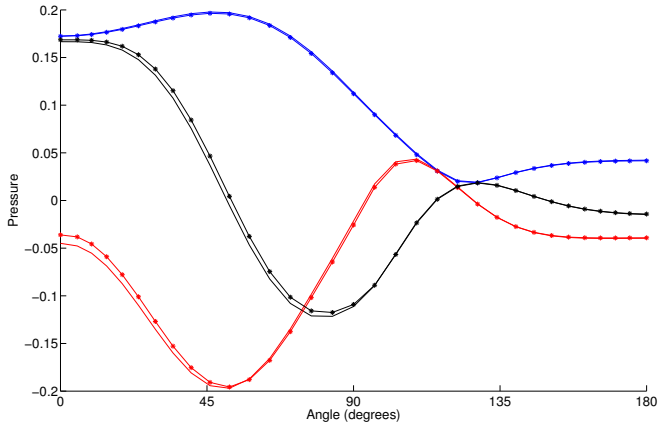

Fig. 3.27. Infinitesimal cylinder radiation with a constant enrichment at 500 Hz with a uniform mean flow $\mathbf{v}_0 = -85m/s\ \mathbf{1}z$, $n_p = 30$, $n_r = 30$: illustration of the analytical and the computed pressure along the interface Γ: absolute (blue), real (red) and imaginary (black) part of the pressure.

- third order functions with $n_p = 8$, $n_r = 8$ $(1126 dofs)$ in figure 3.29.

The relative difference along the interface is plotted on the same figure for these three results (fig. 3.30). We can observe that the best accuracy is reached for high enrichment orders (note that all computations have the same number of unknowns).

We may conclude that the proposed method is verified for convected propagation. We want to warn the reader that we observed that ill-conditioning could lead to a small loss of accuracy (for more informations on the conditioning please refer to section 5.1.3). We observe that the computation with the cubic enrichment of the infinitesimal cylinder radiation at 500 Hz with a uniform mean flow $\mathbf{v}_0 = -85m/s\ \mathbf{1}z$ and a mesh given by $n_p = 12$ and $n_r = 12$ leads to a L^2 relative error (equation 5.1) of 5.1%. The condition number of the system is very high: $cond = 7.7\ 10^{17}$ as it is generally observed for the

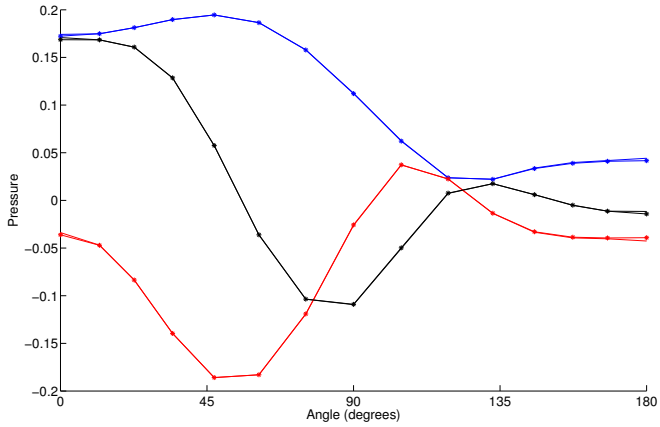

Fig. 3.28. Infinitesimal cylinder radiation with a second order enrichment at 500 Hz with a uniform mean flow $\mathbf{v}_0 = -85m/s\ \mathbf{1}z$, $n_p = 12$, $n_r = 12$: illustration of the analytical and the computed pressure along the interface Γ: absolute (blue), real (red) and imaginary (black) part of the pressure.

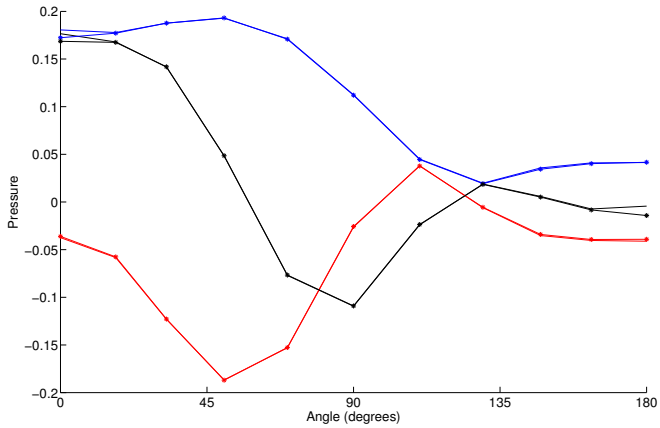

Fig. 3.29. Infinitesimal cylinder radiation with a third order enrichment at 500 Hz with a uniform mean flow $\mathbf{v}_0 = -85m/s\ \mathbf{1}z$, $n_p = 8$, $n_r = 8$: illustration of the analytical and the computed pressure along the interface Γ: absolute (blue), real (red) and imaginary (black) part of the pressure.

Partition of Unity Method (section 5.1.3). We artificially improve the conditionning by adding on the diagonal of the matrix a term proportional to the highest value of the diagonal. This is a correction method classicaly used in preconditionning techniques for solving ill conditionned systems. If this proportion is taken to be 10^{-14} the L^2 relative error drops to 3.37% and to 1.83% for 10^{-10}. Ill-conditioning has a slight negative influence on the accuracy but we note that a basic preconditionning technique allows to reduce the effect of ill conditionning.

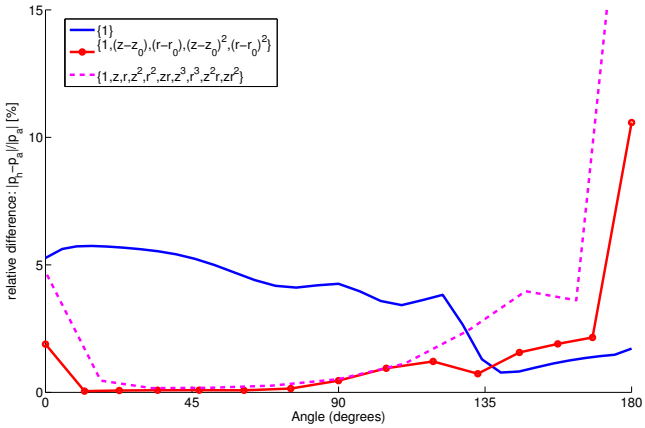

Fig. 3.30. Infinitesimal cylinder radiation at 500 Hz with a uniform mean flow $\mathbf{v}_0 = -85m/s\ \mathbf{1}z$: illustration of the relative difference [%] along the interface Γ. (Some simplifications have been made in the legend. The third order terms $\{x, y, ...\}$ have to be read as $\{(x - x_0), (y - y_0), ...\}$)

References

1. Ph. Bouillard, F. Ihlenburg, Error estimation and adaptivity for the finite element solution in acoustics: 2D and 3D applications, Comput. Methods Appl. Mech. Engrg. 176 (1999) 147-163.
2. F. Ihlenburg, I. Babuška, Dispersion analysis and error estimation of Galerkin finite element methods for the Helmholtz equation, Int. J. Numer. Methods Eng. 38 (1995) 3745-3774.
3. J.T. Oden, S. Prudhomme, L. Demkowicz, A posteriori error estimation for acoustic wave propagation problems, Arch. Comput. Meth. Engng. 12 (2005) 343-389.
4. F. Ihlenburg, I. Babuška, Finite element solution of the Helmholtz equation with high wave number part II : the h-p version of the FEM, SIAM J. Numer. Anal. 34 (1997) 315-358.
5. O.C. Zienkiewicz, Achievements and some unsolved problems of the finite element method, Int. J. Numer. Methods Eng. 47 (2000) 9-28.
6. L.L. Thompson, A review of finite element methods for time-harmonic acoustics, J. Acoust. Soc. Am. 119 (2006) 1315-1330.
7. J.M. Melenk, I. Babuška, The partition of unity finite element method: basic theory and applications, Comput. Methods Appl. Mech. Engrg. 139 (1996) 289-314.
8. I. Babuška, J.M. Melenk, The Partition of Unity Method, Int. J. Numer. Methods Eng. 40 (1997) 727-758.
9. O. Laghrouche, P. Bettess, R. J. Astley, Modeling of short wave diffraction problems using approximating systems of plane waves, Int. J. Numer. Methods Eng. 54 (2002) 1501-1533.
10. Th. Strouboulis, I. Babuška, R. Hidajat, The generalized finite element method for Helmholtz equation: Theory, computation, and open problems, Comput. Methods Appl. Mech. Engrg. 195 (2006) 4711-4731.
11. Th. Strouboulis, R. Hidajat, I. Babuška, The generalized finite element method for Helmholtz equation Part II: Effect of choice of handbook functions, error due to absorbing boundary conditions and its assessment, Comput. Methods Appl. Mech. Engrg. 197 (2008) 364-380.
12. Th. Strouboulis, K. Copps, I. Babuška, The generalized finite element method, Comput. Methods Appl. Mech. Engrg. 190 (2001) 4081-4193.
13. Th. Strouboulis, I. Babuška, K. Copps, The design and analysis of the generalized finite element method, Comput. Methods Appl. Mech. Engrg. 181 (2000) 43-69.
14. C. Farhat, I. Harari, L.P. Franca, The discontinuous enrichment method, Comput. Methods Appl. Mech. Engrg. 190 (2001) 6455-6479.
15. B. Pluymers, W. Desmet, D. Vandepitte, P. Sas, Application of an efficient wave-based prediction technique for the analysis of vibro-acoustic radiation problems, J. Comput. Appl. Math. 168 (2004) 353-364.
16. P. Gamallo, R.J. Astley, A comparison of two Trefftz-type methods: The ultraweak variational formulation and the least-squares method, for solving shortwave 2-D Helmholtz problems, Int. J. Numer. Methods Eng. 71 (2007) 406-432.
17. P. Gamallo, R.J. Astley, The partition of unity finite element method for short wave acoustic propagation on non-uniform potential flows, Int. J. Numer. Methods Eng. 65 (2006) 425-444.
18. T. Huttunen, P. Gamallo, R.J. Astley, Comparison of two wave element methods for the Helmholtz problem, Commun. Numer. Meth. Engng. Article in Press (2008) doi:10.1002/cnm1102.
19. T. Huttunen, P. Monk, J.P. Kaipio, Computational aspects of the ultra weak variational formulation, J. Comput. Phys. 182 (2002) 27-46.
20. T. Huttunen, J.P. Kaipio, P. Monk, An ultra weak method for acoustic fluid-solid interaction, J. Comput. Appl Math. 213 (2008) 166-185.

21. P. Monk, D.-Q. Wang, A least squares method for the Helmholtz equation, Comput. Methods Appl. Mech. Engrg. 175 (1999) 121-136.
22. R. Sevilla, S. Fernández-Méndez, A. Huerta, NURBS-enhanced finite element method (NEFEM), Int. J. Numer. Methods Eng. Early ViewW (2008) doi: 10.1002/nme.2311
23. E. Chadwick, P. Bettess, O. Laghrouche, Diffraction of short waves modeled using new mapped wave envelope finite and infinite elements, Int. J. Numer. Methods Eng. 45 (1999) 335-354.
24. E. De Bel, P. Villon, Ph. Bouillard, Forced vibrations in the medium frequency range solved by a partition of unity method with local information, Int. J. Numer. Methods Eng. 162 (2004) 1105-1126.
25. L. Hazard, Ph. Bouillard, Structural dynamics of viscoelastic sandwich plates by the partition of unity finite element method, Comput. Methods Appl. Mech. Engrg. 196 (2007) 4101-4116.
26. T.J.R. Hughes, J.A. Cotrell, Y. Bazilevs, Isogeometric analysis: CAD, finite elements, NURBS, exact geometry and mesh refinement, Comput. Methods Appl. Mech. Engrg. 194 (2005) 4135-4195.
27. B. Szabó, A. Düster, E. Rank, The p-version of the finite element method, in: E. Stein, R. de Borst, T.J.R. Hughes (Eds.), Fundamentals, Encyclopedia of Computational Mechanics, vol. 1, Wiley, New York, 2004 (Chapter 5).
28. R.J. Astley, P. Gamallo, Special short wave elements for flow acoustics, Comput. Methods Appl. Mech. Engrg. 194 (2005) 341-353.
29. R.J. Astley, P. Gamallo, The Partition of Unity Finite Element Method for Short Wave Acoustic Propagation on Non-uniform Potential Flows, Int. J. Numer. Methods Eng. 65 (2006) 425-444.
30. R.J. Astley, G.J. Macaulay, J.-P. Coyette, L. Cremers, Three-dimensional wave-envelope elements of variable order for acoustic radiation and scattering. Part I. Formulation in the frequency domain, J. Acoust. Soc. Am. 103 (1998) 49-63.
31. R.J. Astley, J.-P. Coyette, Conditioning of infinite element schemes for wave problems, Commun. Numer. Meth. Engng. 17 (2001) 31-41.
32. D. Dreyer, O. von Estorff, Improved conditioning of infinite elements for exterior acoustics, Int. J. Numer. Methods Eng. 58 (2003) 933-953.
33. J.J. Shirron, I. Babuška, A comparison of approximate boundary conditions and infinite element methods for exterior Helmholtz problems, Comput. Methods Appl. Mech. Engrg. 164 (1998) 121-139
34. D. Dreyer, Efficient infinite elements for exterior acoustics, PhD thesis, Shaker Verlag, Aachen, 2004.
35. W. Eversman, Mapped infinite wave envelope elements for acoustic radiation in a uniformly moving medium, J. Sound Vib. 224 (1999) 665-687.
36. S.J. Rienstra, W. Eversman, A numerical comparison between the multiple-scales and finite-element solution for sound propagation in lined flow ducts, J. Fluid Mech. 437 (2001) 367-384.
37. S.J. Rienstra, Sound transmission in slowly varying circular and annular lined ducts with flow, J. Fluid Mech. 380 (1999) 279-296.
38. S.J. Rienstra, The Webster equation revisited, 8th AIAA/CEAS Aeroacoustic conference (2002) AIAA 2002-2520.
39. M.K. Myers, On the acoustic boundary condition in the presence of flow, J. Sound Vib. 71 (1980) 429-434.
40. T. Mertens, Meshless modeling of acoustic radiation in infinite domains, Travail de spécialisation, Université Libre de Bruxelles (U.L.B.), 2005.
41. W. Eversman, The boundary condition at an impedance wall in a non-uniform duct with potential mean flow, J. Sound Vib. 246 (2001) 63-69.
42. B. Regan, J. Eaton, Modeling the influence of acoustic liner non-uniformities on duct modes, J. Sound Vib. 219 (1999) 859-879.
43. H.-S. Oh, J.G. Kim, W.-T. Hong, The Piecewise Polynomial Partition of Unity Functions for the Generalized Finite Element Methods, Comput. Methods Appl. Mech. Engrg. Accepted manuscript (2008), doi: 10.1016/j.cma.2008.02.035.
44. Free Field Technologies, Actran user's manual, http://fft.be.
45. University of Florida, Department of Computer and Information Science and Engineering, http://www.cise.ufl.edu/research/sparse/umfpack/
46. T.A. Davis, A column pre-ordering strategy for the unsymmetric-pattern multifrontal method, ACM Transactions on Mathematical Software 30 (2004) 165-195.
47. T.A. Davis, Algorithm 832: UMFPACK, an unsymmetric-pattern multifrontal method, ACM Transactions on Mathematical Software 30 (2004) 196-199.
48. T.A. Davis and I.S. Duff, A combined unifrontal/multifrontal method for unsymmetric sparse matrices, ACM Transactions on Mathematical Software 25 (1999) 1-19.

49. T.A. Davis and I.S. Duff, An unsymmetric-pattern multifrontal method for sparse LU factorization, SIAM Journal on Matrix Analysis and Applications 18 (1997) 140-158.
50. A. Hirschberg, S.W. Rienstra, An introduction to aeroacoustics, Eindhoven University of Technology (2004).
51. G. Warzée, Mécanique des solides et des fluides, Université Libre de Bruxelles (2005).
52. M.J. Crocker, Handbook of acoustics, Wiley-Interscience, New York (1998).
53. R. Sugimoto, P. Bettess, J. Trevelyan, A numerical integration scheme for special quadrilateral finite elements for the helmholtz equation, Commun. Numer. Meth. Engng. 19 (2003) 233-245.
54. G. Gabard, R.J. Astley, A computational mode-matching approach for sound propagation in three-dimensional ducts with flow, J. Sound Vib. Article in Press (2008) doi:10.1016/j.jsv.2008.02.015.
55. C. Farhat, I. Harari, U. Hetmaniuk, A discontinuous Galerkin method with Lagrange multipliers for the solution of Helmholtz problems in the mid-frequency regime, Comput. Methods Appl. Mech. Engrg. 192 (2003) 1389-1419.
56. C.L. Morfey, Acoustic energy in non-uniform flows, J. Sound Vib. 14 (1971) 159-170.
57. F. Magoules, I. Harari (editors), Special issue on Absorbing Boundary Conditions, Comput. Methods Appl. Mech. Engrg. 195 (2006) 3354-3902.
58. M. Fischer, U. Gauger, L. Gaul, A multipole Galerkin boundary element method for acoustics, Engineering Analysis with Boundary Elements 28 (2004) 155-162.
59. J.-P. Bérenger, Three-dimensional Perfectly Matched Layer for the absorption of electromagnetic waves, J. Comput. Phys. 127 (1996) 363-379.
60. C. Michler, L. Demkowicz, J. Kurtz, D. Pardo, Improving the performance of Perfectly Matched Layers by means of hp-adaptivity, Numerical Methods for Partial Differential Equations 23 (2007) 832-858.
61. A. Bayliss, E. Turkel, Radiation boundary conditions for wave-like equations, Comm. Pure Appl. Math. 33 (1980) 707-725.
62. B. Engquist, A. Majda, Radiation boundary conditions for acoustic and elastic wave calculations, Comm. Pure Appl. Math. 32 (1979) 313-357.
63. K. Feng, Finite element method and natural boundary reduction, Proceedings of the International Congress of Mathematicians, Warsaw (1983) 1439-1453.
64. D. Givoli, B. Neta, High-order non-reflecting boundary scheme for time-dependent waves, J. Comput. Phys. 186 (2003) 24-46.
65. T. Hagstrom, A. Mar-Or, D. Givoli, High-order local absorbing conditions for the wave equation: Extensions and improvements, J. Comput. Phys. 227 (2008) 3322-3357.
66. T. Hagstrom, T. Warburton, A new auxiliary variable formulation of high-order local radiation boundary conditions: corner compatibility conditions and extensions to first order systems, Wave Motion 39 (2004) 327-338.
67. A. Hirschberg, S.W. Rienstra, An introduction to aeroacoustics, Eindhoven university of technology (2004).
68. V. Lacroix, Ph. Bouillard, P. Villon, An iterative defect-correction type meshless method for acoustics, Int. J. Numer. Meth. Engng 57 (2003) 2131-2146.
69. T. Mertens, P. Gamallo, R. J. Astley, Ph. Bouillard, A mapped finite and infinite partition of unity method for convected acoustic radiation in axisymmetric domains, Comput. Methods Appl. Mech. Engrg. 197 (2008) 4273-4283.
70. G. Gabard, Discontinuous Galerkin methods with plane waves for time harmonic problems, J. Comput. Phys. 225 (2007) 1961-1984.
71. L. Hazard, Design of viscoelastic damping for vibration and noise control: modeling, experiments and optimisation, PhD thesis, Univesité Libre de Bruxelles (2007).
72. G. Gabard, R.J. Astley, M. Ben Tahar, Stability and accuracy of finite element methods for flow acoustics. I: general theory and application to one-dimensional propagation, Int. J. Numer. Meth. Eng. 63, (2005) 947-973.
73. G. Gabard, R.J. Astley, M. Ben Tahar, Stability and accuracy of finite element methods for flow acoustics. II: Two-dimensional effects, Int. J. Numer. Meth. Eng. 63 (2005) 974-987.
74. A. Goldstein, Steady state unfocused circular aperture beam patterns in non attenuating and attenuating fluids, J. Acoust. Soc. Am. 115 (2004) 99-110.
75. T. Douglas Mast, F. Yu, Simplified expansions for radiation from baffled circular piston, J. Acoust. Soc. Am. 118 (2005) 3457-3464.
76. T. Hasegawa, N. Inoue, K Matsuzawa, A new rigorous expansion for the velocity potential of a circular piston source, J. Acoust. Soc. Am. 74 (1983) 1044-1047.
77. R.J. Astley, A finite element, wave envelope formulation for acoustical radiation in moving flows, J. Sound Vib. 103 (1985) 471-485.
78. J.M. Tyler, T.G. Sofrin, Axial flow compressor noise studies, SAE Transactions 70 (1962) 309-332.

79. M.C. Duta, M.B. Giles, A three-dimensional hybrid finite element/spectral analysis of noise radiation from turbofan inlets, J. Sound Vib. 296 (2006) 623-642.
80. H.H. Brouwer, S.W. Rienstra, Aeroacoustics research in Europe: The CEAS-ASC report on 2007 highlights, J. Sound Vib. Article in Press (2008) doi:10.1016/j.jsv.2008.07.020.
81. http://en.wikipedia.org/wiki/Aircraft_noise, 4th September 2008.
82. Y. Park, S. Kim, S. Lee, C. Cheong, Numerical investigation on radiation characteristics of discrete-frequency noise from scarf and scoop aero-intakes, Appl. Acoust. Article in press (2008) doi:10.1016/j.apacoust.2007.09.005.
83. General Electric Company, http://www.ge.com, http://www.turbokart.com/about_ge90.htm, 4th September 2008.
84. R.J. Astley, J.A. Hamilton, Modeling tone propagation from turbofan inlets - The effect of extended lip liner, AIAA paper 2002-2449 (2002).
85. V. Decouvreur, Updating acoustic models: a constitutive relation error approach, PhD thesis, Université Libre de Bruxelles (2008).
86. P.A. Nelson, O. Kirkeby, T. Takeuchi, and H. Hamada, Sound fields for the production of virtual acoustic images, Letters to the editor, J. Sound Vib. 204 (1999) 386-396.
87. Y. Reymen, W. De Roeck , G. Rubio, M. Bealmans, W. Desmet, A 3D Discontinuous Galerkin Method for aeroacoustic propagation, Proceedings of the 12th International Congress on Sound and Vibration 2005.
88. G. Gabard, Exact integration of polynomial-exponential products with an application to wave based numerical methods, Commun. Numer. Meth. Engng (2008) doi: 10.1002/cnm.1123.
89. New York University, http://math.nyu.edu/faculty/greengar/shortcourse_fmm.pdf, 1st december 2008.